Cyano-tryptophans as dual infrared and fluorescence spectroscopic labels to assess structural dynamics in proteins

van Wilderen, L J G W; Brunst, H; Gustmann, H; Wachtveitl, J; Broos, J; Bredenbeck, J

Published in:
PPCP : Physical Chemistry Chemical Physics

DOI:
10.1039/c8cp00846a

Publication date:
2018

PCCP

PAPER

View Article Online
View Journal | View Issue

Cite this: *Phys. Chem. Chem. Phys.*, 2018, **20**, 19906

Cyano-tryptophans as dual infrared and fluorescence spectroscopic labels to assess structural dynamics in proteins†

L. J. G. W. van Wilderen, [a] H. Brunst, [a] H. Gustmann, [b] J. Wachtveitl, [b] J. Broos[c] and J. Bredenbeck *[a]

The steady state and time-resolved fluorescence and infrared (IR) properties of 4- and 5-cyanotryptophan (CNTrp) are investigated and compared, and the tryptophan (Trp) analogs are found to be very attractive to study structural and dynamic properties of proteins. The position of the nitrile substitution as well as the solvent environment influences the spectroscopic properties (solvatochromism). Similar to native Trp, electronic (nanosecond) lifetime and emission spectra are modulated by the environment, making CNTrps attractive fluorescent probes to study the structural dynamics of proteins in complex media. The nitrile absorption in the IR region can provide local structural information as it responds sensitively to changes in electrostatics and hydrogen bond (HB) interactions. Importantly, we find that 4CNTrp exhibits a single absorption in the nitrile stretch region, while the model compound 4CN-indole (4CNI) shows two. Even though the spectrum of the model compound is perturbed by a Fermi resonance, we find that 4CNTrp itself is a useful IR label. Moreover, if the nitrile group is substituted at the 5 position, the Trp analog predominantly reports on its HB status. Because the current literature on similar compounds is too limited for a detailed solvatochromic analysis, we extend the available data significantly. Only now are microscopic details such as the mentioned sensitivity to electrostatics coming to light. The vibrational lifetime of the CN moiety (acting on a picosecond time scale in contrast to the nanosecond time scale for fluorescent emission) allows for its application in 2D-IR spectroscopy in the low picosecond range. Taken together, the benefits of CNTrps are that they absorb and emit separately from the naturally occurring Trp and that in these dual fluorescence/vibrational labels, observables of IR and fluorescence spectroscopy are modulated differently by their surroundings. Because IR absorption and fluorescence operate on different time and length scales, they thus provide complementary structural information.

Received 5th February 2018,
Accepted 25th June 2018

DOI: 10.1039/c8cp00846a

rsc.li/pccp

Introduction

The fluorescence of Trp (*i.e.* in terms of intensity, lifetime, and wavelength) is strongly modulated by its local electrostatics, structure and hydrogen bond (HB) partners.[1–4] Therefore, it is widely used as a marker for changes in the hydration status[5] and conformation[6,7] of a protein. Its fluorescence (it absorbs at around 280 nm and emits at around 350 nm) has, for instance, been used *via* Förster Resonance Energy Transfer (FRET) methods to gain distance information on length scales of 1–10 nm.[8–10] Here, we study cyano-tryptophans (see Fig. 1) as potential protein labels, having a nitrile group functioning as an additional IR label. A cyano group on a different amino acid such as phenylanaline[11–15] has, for instance, been used as a direct IR and fluorescence label in a protein,[14] or to perturb the fluorescence of GFP's chromophores while simultaneously reporting

[a] *Institute of Biophysics, Johann-Wolfgang-Goethe Universität, Frankfurt am Main, Germany. E-mail: bredenbeck@biophysik.uni-frankfurt.de*
[b] *Institute of Physical and Theoretical Chemistry, Johann-Wolfgang-Goethe Universität, Frankfurt am Main, Germany*
[c] *Laboratory of Biophysical Chemistry and GBB (Groningen Biomolecular Science and Biotechnology Institute), University of Groningen, Nijenborgh 7, 9747 AG Groningen, The Netherlands*

† Electronic supplementary information (ESI) available: Raw data of the ultrafast infrared measurements as well as an extensive UV/vis characterization are presented. See DOI: 10.1039/c8cp00846a

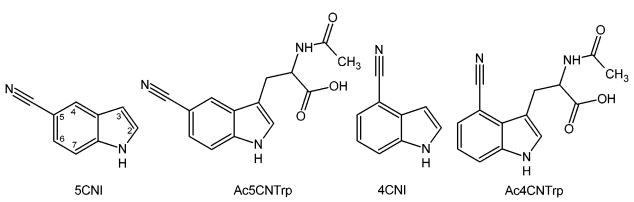

Fig. 1 Model compounds 5CNI, Ac5CNTrp, 4CNI and Ac4CNTrp. The atom numbering is given for 5CNI.

on the local electrostatics and HB interactions *via* the cyano group's IR properties.[11] Many other natural and unnatural protein labels are currently available,[16,17] illustrating the vast potential for investigations on protein structures.

A previous study exploited the use of 5CNTrp as a fluorescence and IR protein label.[16,18,19] Very recently, Hilaire *et al.*[20] reported on 4CNTrp, showing a strong absorption of 4CNTrp at wavelengths >300 nm. Together with attractive fluorescence properties like a high quantum yield and good photostability, this gives 4CNTrp potential as an attractive protein fluorescence probe. Nitrile groups have strong IR absorption cross sections, are spectrally isolated from water and protein absorption bands, and their central wavenumber is sensitive to changes in local electrostatics and HB interactions.[21] The possibility of the dual use of 5CNTrp as a fluorescence and IR protein label has already been pointed out.[18] The molar absorptivity of the studied compounds is assumed to be similar to Trp and those of previously reported structurally related compounds,[22] *i.e.* about 5000 M^{-1} cm^{-1} at the maximum absorption in the UV region, and about 160 M^{-1} cm^{-1} in the infrared region.[23] Here, we show that 4CNTrp can be used both as a dual fluorescence and IR label, extending the biochemical toolbox and investigating and comparing the spectroscopic properties of the two CNTrps.[23–26] Repositioning the CN group is useful as its spectroscopic properties are enhanced (*e.g.* fluorescence quantum yield and lifetime) and highly directional, thus a different microenvironment is probed. In order to be able to understand the response of the label for future use inside a protein environment, the IR and fluorescence spectral shifts (*i.e.* solvatochromism) of the labels as well as those of the CN-indole model compounds are characterized in this work using a set of solvents having different polarities and HB interactions. These compounds, shown in Fig. 1, are 4CN-indole (4CNI), 5CN-indole (5CNI), *N*-acetyl-4CN-Trp (Ac4CNTrp) and *N*-acetyl-5CN-Trp (Ac5CNTrp). The occurring spectral shifts in both regions of the electromagnetic spectrum are described by different theoretical models and discussed.

Experimental

Amino acid preparation

DL *N*-acetyl-4CN-Trp and DL *N*-acetyl-5CN-Trp were prepared *via* condensation of 4CNI or 5CNI with serine in the presence of acetic acid anhydride and acetic acid essentially as described before.[27,28]

Solvents

All solvents (Sigma Aldrich): acetonitrile, chloroform, dichloromethane (DCM), dimethylformamide (DMF), dimethyl sulfoxide (DMSO), perchloroethylene (PCE), tetrahydrofuran (THF), 1,1,1,3,3,3-hexafluoro-2-propanol (HFIP), methanol and 2,2,2-trifluoroethanol (TFE) were used as received.

Infrared spectroscopy

Steady-state IR measurements were done on a nitrogen-purged Bruker Tensor 27 FTIR (Bruker, Billerica, USA) equipped with an MCT detector and 64 scans were made to collect each averaged spectrum, except the measurement of 5CNI in water, which was averaged over 256 scans. A flow cell[29] having a Polytetrafluorethylen (PTFE) spacer of 50 μm thickness determines the optical path length. The solutions had a concentration between 17 mM and 50 mM when solubility was sufficiently high. In H_2O, solubility of all samples was poor. The solubility was also a limiting factor for 4CNI in PCE, Ac4CNTrp in acetonitrile and Ac5cnTrp in chloroform and PCE. For these samples, saturated solutions with estimated concentrations down to 0.6 mM for Ac5CNTrp in PCE have been used, limiting the signal to a noise ratio of the spectra. Ac4CNTrp does not dissolve in PCE. A third- to seventh-order polynomial function was used to correct for the broad baseline underlying the nitrile feature. The spectra in water were collected by using an added amount of DMSO (10 vol%) to increase the solubility. Because of limited sample availability, not all solvents were used for the Trp analogs. The used solvents were chosen to obtain the largest spread in the solvent field.

Ultrafast IR experiments were performed by using a Ti:sapphire regenerative amplifier (4.5 mJ, 800 nm, 90 fs, 1 kHz, Mira Legend Elite HE of Coherent, Santa Clara, USA) that pumped two home-built optical parametric amplifiers (OPAs). One OPA was used to generate IR probe pulses by difference frequency generation (DFG) of the signal and idler in $AgGaS_2$. The other OPA generated broadband IR pump pulses (about 9 μJ). The spectra were recorded on a 2 × 32 pixel mercury cadmium telluride (MCT) detector (Infrared Associates, USA). The delay of the IR pump pulse was controlled by a translation stage. A chopper was used to collect 'pump-on' and 'pump-off' signals. The signal at −20 ps was subtracted as a background. The instrument response was about 150 fs. The measurements were done on a sample cell consisting of two CaF_2 windows, separated by a PTFE spacer (250 μm thick in THF and DMSO, at about 10–30 mM concentration, and 50 μm in H_2O, at saturated concentration). A global analysis was performed on the ultrafast data by using the Globe Toolbox[30] to extract the lifetimes from a sum of exponential functions fitted to the data.

UV/visible spectroscopy

The UV/visible spectra were measured by using a Hitachi U 2000 or Jasco V-650 spectrophotometer (JASCO Deutschland GmbH, Pfungstadt, Germany) at room temperature using either a 1 mm cuvette, a 10 mm cuvette or a flow cell.[29] The solvent spectrum was subtracted as a background and the resulting spectra (2 nm resolution) were corrected for a constant offset. The fluorescence spectra were measured either by using a Perkin Elmer LS 55 spectrometer using a 10 mm cuvette, or a Jasco FP-8500 spectrometer (JASCO Deutschland GmbH, Pfungstadt, Germany) using a 10 mm × 4 mm UV-grade quartz cuvette (29-F/Q/10, Starna GmbH, Pfungstadt, Germany). The solvent spectrum was subtracted as a background. The solutions were freshly prepared to have an OD of about 0.1 at the excitation wavelength of 310 nm (corresponding to a concentration of a few tens to 200 μM). The averaged (10 scans) emission was measured from 250–550 nm in 0.5 nm steps,

and scatter of the solvent was subtracted by using an independent measurement.

For the absolute quantum yield determination, a Jasco FP-8500 spectrometer with a 100 mm integrating sphere (Jasco ILF-835) was used. For all fluorescence quantum yield measurements, the excitation wavelength of 310 nm and a 10 mm × 4 mm UV-grade quartz cuvette (29-F/Q/10, Starna GmbH) were used. The data were corrected for spectral characteristics of the equipment (*i.e.* detector correction).

Time-resolved fluorescence measurements were performed with a time-correlated single photon counting (TCSPC) setup, which was described earlier.[31] As an excitation source, a PicoQuant PLS 310 pulsed laser diode (PicoQuant GmbH, Berlin, Germany; producing 500–800 ps pulses at 310 nm) was used, driven by a PDL 800-D diode driver. The solutions were freshly prepared to have an OD of about 0.1 at 310 nm, similar to the recording of emission spectra. The sample was contained in a 10 mm × 4 mm UV-grade quartz cuvette (29-F/Q/10, Starna GmbH). The sample temperature was held constant at 20 °C. A 320 nm high pass filter (N-WG-320, Schott AG, Mainz, Germany) was used to block scattered light, and the emitted light with wavelengths >320 nm was integrated. Contributions of Raman scatter in the data collected in H_2O (as well as for Ac4CNTrp in TFE) were minimized for the samples exhibiting small fluorescence signals by using additional optical filters (excitation filter: 310 nm UG 11; emission filters: 2 × 375 nm GG (green glass), 385 nm GG, all from Schott AG, Mainz, Germany). A TiO_2 suspension in each solvent was used as a scatter sample to determine the instrument response function (IRF). For the analysis, the data were fitted with a sum of exponentials after deconvolution with the IRF with the help of the FluoFit Pro 4.6 (PicoQuant) software. All UV/vis data in H_2O were collected with 10% DMSO, except for the absorption spectrum of 5CNI as well as all 4CNI data, which were measured by using 10% methanol to increase the solubility.

Results and discussion

Infrared properties

The solvent dependence of the steady-state IR absorption spectrum of 5CNI is shown in Fig. 2A. Similar to our previous study on methyl thiocyanate[32,33] and that of 3-methyl-5-cyanoindole by Zhang *et al.*,[34] blueshifts are observed for apolar as well as HB forming solvents. Changing the solvent from apolar perchloroethylene (PCE; dark blue) to polar dimethyl sulfoxide (DMSO; orange) leads to a redshift of the nitrile stretch mode. Changing from the non-HB forming solvent DMSO (orange) to water (black) leads to a blueshift.

The solvatochromic shifts may seem counter-intuitive as the polarity is usually high for HB forming solvents, yet HB formation causes a shift in a different direction than when the polarity is increased. DFT computations on CN in nitriles and thiocyanates have shown that field components other than that along the cyanide bond need to be taken into account to explain such effects.[21] Changing the HB geometry can cause either a blueshift (a linear HB geometry) or a redshift (a non-linear one). Our data thus support a linear configuration for 5CNI and the other compounds as well, which show similar shifts upon HB formation. Table 1 lists all (fitted) central wavenumbers and bandwidths at fwhm (full width at half maximum). Table S1 (ESI†) also shows the corresponding errors.

The spectra of 4CNI are distinctly different from 5CNI, as they do not show a single but two absorption bands (see Fig. 2C), in agreement with previous observations.[35] We therefore at first

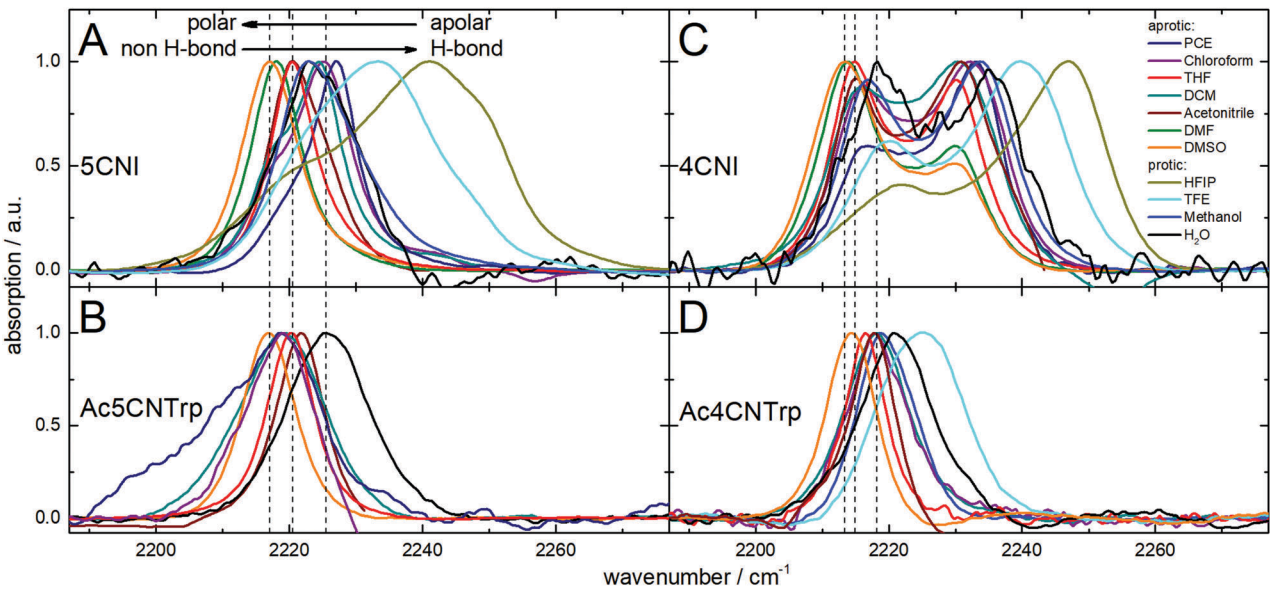

Fig. 2 Solvent dependence of the normalized nitrile absorption band of the 5CNI (panel A), Ac5CNTrp (panel B), 4CNI (panel C) and Ac4CNTrp (panel D) model compounds. The general trend, depicted by arrows in panel A, is seen in all panels (sharing the same abscissa and legend). Some spectra are noisy, caused by poor solubility. The vertical dashed lines serve as guides to the eye, marking the maxima of DMSO, THF and H_2O in the top panels. The central wavenumbers and widths of each band are given in Table 1.

Table 1 Central wavenumber ν_c and fwhm of the nitrile vibration of 5CNI, Ac5CNTrp, 4CNI and Ac4CNTrp in different environments. The listed values are a result of Lorentzian fits to the data shown in Fig. 2. Using a Gaussian or a Voigt profile produced nearly identical results. Table S1 (ESI) also shows the corresponding errors

	Compound	5CNI	Ac5CNTrp	4CNI		Ac4CNTrp
Solvent	Dielectric constant ε[36]	ν_c (fwhm)/cm^{-1}	ν_c (fwhm)/cm^{-1}	ν_c (fwhm) peak 1/cm^{-1}	ν_c (fwhm) peak 2/cm^{-1}	ν_c (fwhm)/cm^{-1}
Aprotic						
PCE	2.27	2226(9)	2219(12)	2218(12)	2233(10)	
Chloroform	4.81	2224(12)	2219(15)	2217(11)	2232(12)	2218(10)
THF	7.52	2221(8)[a]	2220(8)[b]	2215(9)[c]	2230(10)[c]	2216(7)
DCM	8.93	2223(12)	2219(15)	2217(13)[c]	2230(12)[c]	2218(11)
Acetonitrile	36.64	2221(10)	2222(9)	2215(9)	2230(14)	2217(10)
DMF	38.25	2218(8)		2214(10)[c]	2229(11)[c]	
DMSO	47.24	2217(9)	2217(9)	2214(11)[c]	2229(12)[c]	2214(7)
Protic						
HFIP	16.70	2225(26)/2242(21)		2223(25)	2246(14)	
TFE	27.68	2232(23)		2220(13)[c]	2240(15)[c]	2225(13)
Methanol	33.0	2224(13)		2217(10)[c]	2233(12)[c]	2219(9)
H_2O	80.2	2224(13)[a]	2226(13)[b]	2219(12)	2235(12)	2221(12)

[a] Previously reported at 2220(8) cm^{-1} in THF, 2224(18) cm^{-1} in a H_2O/MeOH (95/5) mixture.[23] [b] Previously reported for Fmoc-L-5CNTrp in THF and H_2O/THF (60/40) at 2220 cm^{-1}. [c] These values are consistent with previously reported values (deviating by 0.7 cm^{-1} at most).[35]

were pessimistic about the potential use of Ac4CNTrp as an IR label. Interestingly, the second peak of 4CNI disappeared for Ac4CNTrp (see Fig. 2D), greatly simplifying the line shape, and thus the interpretation of the data. The second peak is most likely caused by a Fermi resonance, which vanishes upon substitution. Supporting evidence comes from DFT computations, which only show one vibration in the nitrile region, in addition to experimental evidence for the coupling of both bands (2D-IR spectroscopy reveals instantaneous cross-peaks between the two bands in isopropanol[35]). A low wavenumber mode at around 1125 cm^{-1} apparently changed its wavenumber due to an additional amino-acid chain, shifting its first overtone away from the nitrile stretch mode. Polarized 2D-IR experiments, isotope labelling, or anharmonic frequency computations could provide further proof for the assignment to a Fermi resonance. We conclude that Ac4CNTrp can serve as an attractive and 'simple' IR probe as it exhibits one band only. It is also noted that the spectrum of 5CNI in the protic solvent HFIP shows at least two peaks, which may be similarly explained by an occurring Fermi resonance (Fig. 2A, dark yellow). However, because this seems to be the only affected spectrum, we assign these two bands to different HB states (with the low wavenumber band corresponding to the non-HB species, as it fits best to the Onsager model for aprotic solvents described below).

In protic solvents, both 5CNI and 4CNI show the largest fwhm values, indicating inhomogeneous broadening due to HB formation. Compare for instance, 4CNI in HFIP (both bands have large fwhm values, being 14 cm^{-1} and 25 cm^{-1}) to that obtained in THF (both bands have similar widths, being 9 cm^{-1} and 10 cm^{-1}). Similar bandwidth effects are also found for other nitriles.[32–34]

The solvatochromic effect can be described by Kamlet–Taft empirical solvatochromic theory, which uses (fixed) solvent-dependent parameters to describe the observed spectral shifts.[37,38] Using three α, β, and π^* parameters (characterizing the solvent's HB donor acidity, HB acceptor basicity and solvent polarity/polarizability, respectively; see Table S3, ESI†), the model compounds show a linear relationship, even for each of the Fermi resonance-splitted bands (Fig. 3). A fit to the function $\Delta\nu = \nu_0 + a\cdot\alpha + b\cdot\beta + p\cdot\pi^*$ for each compound results in the prefactors listed in Table 2. The linear dependence of all compounds not only demonstrates the validity of the Kamlet–Taft model, but also provides an internal consistency check of all measured data, as shown in Fig. 3, panels A–E.

The R^2 values are close to 1 for this linear model and the linear dependencies are helpful in determining frequency shifts in other solvents if their Kamlet–Taft parameters are known. The physical meaning of the Kamlet–Taft parameters, however, is not very well defined. The modelled wavenumber shift is assumed to be induced by a homogeneous environment. In proteins, the micro-environment of the label is typically rather inhomogeneous, consisting of a relatively stable scaffold formed by many amino acids, each having their own polarity and HB forming characteristics. A more physical picture can be obtained by the Onsager reaction field model ($\Delta\nu_{Obs} = -\vec{F}_{Onsager} f \Delta\vec{\mu}_{solute}$, where $\Delta\nu_{Obs}$ is the observed spectral shift with respect to the gas phase, $\Delta\vec{\mu}_{solute}$ is the linear Stark tuning rate, and f is a local field correction factor[39]), where the spherical solute's dipole moment reacts to the solvent field $\left(\vec{F}_{Onsager}\right)$.[40,41] Although this approach models the underlying physics, it also describes a homogeneous environment, but in contrast to the Kamlet–Taft model above, it explicitly includes electrostatics. Because HB interactions are not included in this simplified model, only the aprotic solvents fit to a straight line ($\vec{F}_{Onsager}$ is taken to be proportional to the dimensionless macroscopic Onsager factor $2(\varepsilon-1)(n^2-2)/(3(2\varepsilon-n^2))$, where ε is the dielectric constant of the solvent, and n is the refractive index of the solute, which is taken to be $n_{Trp} = 1.754$[42] for all compounds). It is interesting to note that the proportionality constant between the field and the observed frequency shift $f\Delta\vec{\mu}_{solute}$ of both peaks of 4CNI is similar, and that it changes for the 5CN analogs from

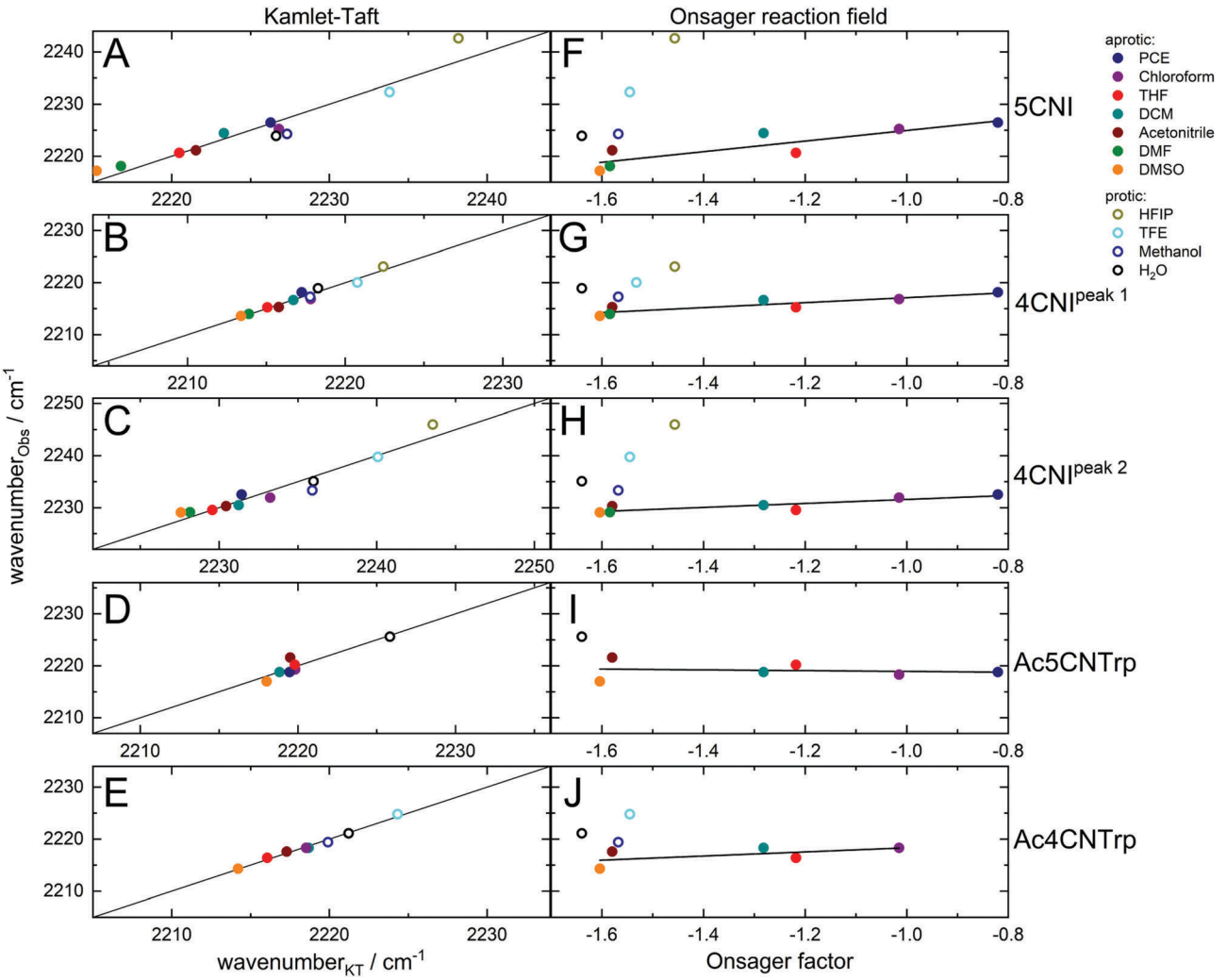

Fig. 3 The observed solvent-dependent frequency shifts ($wavenumber_{Obs}$) are predicted by the Kamlet–Taft (*i.e.* as function of $wavenumber_{KT}$; see panels A–E) and Onsager solvent reaction field (panels F–J). For 5CNI in HFIP, only the high wavenumber band is used. The black lines in panels A–E represent the diagonal, the ones in panels F–J represent a linear fit to the aprotic solvents only. All panels share the same total wavenumber range, allowing the induced spread in observed central wavenumbers to be easily discerned and compared. All panels share the same legend. The protic solvents have open symbols, the aprotic solvents have closed ones.

Table 2 Fit parameters resulting from applying the Kamlet–Taft solvatochromic relationship and the Onsager reaction field model to the IR data of the model compounds. The goodness-of-fit (R^2) as well as the standard deviation (in brackets) are included. Table S3 (ESI) shows the used Kamlet–Taft solvent parameters

	Kamlet–Taft parameters					Onsager model	
Compound	*A*	*B*	*p*	ν_0/cm^{-1}	R^2	$f\Delta\vec{\mu}_{solute}$	R^2
5CNI	8 (2)	−5 (4)	−10 (3)	2229.0	0.94	10 (3)	0.77
Ac5CNTrp	9 (2)	4 (3)	−6 (2)	2221.2	0.86	−1 (3)	0.02
4CNI$^{peak\ 1}$	3.1 (0.3)	−2.9 (0.7)	−2.8 (0.5)	2218.3	0.97	5 (1)	0.82
4CNI$^{peak\ 2}$	6.8 (0.8)	−2 (2)	−4 (1)	2233.2	0.93	4 (1)	0.77
Ac4CNTrp	4.5 (0.3)	−3.5 (0.6)	−2.6 (0.4)	2219.5	0.98	4 (3)	0.35
MeSCN[32,33]	7.6 (0.8)	−8 (2)	−4 (3)	2164.9	0.94	7 (2)	0.79

high for 5CNI to essentially zero for Ac5CNTrp. This is not likely to be caused by differences in refractive index between the structurally-related compounds, as a simple calculation reveals that a deviation of 10% in refractive index (indole deviates by 7%[43]) leads to a change of about 20% in $f\Delta\vec{\mu}_{solute}$, and not to a cancellation. Why the additional substitution induced an insensitivity to electrostatics in Ac4CNTrp but not in Ac5CNTrp remains to be investigated. A clue may however come from Table 2, where it is interesting to note that there seems to be a correlation between the Kamlet–Taft parameter *b* and $f\Delta\vec{\mu}_{solute}$. Strongly negative *b* values tend to lead to high values for $f\Delta\vec{\mu}_{solute}$. Only for Ac5CNTrp a positive *b* value is found, corresponding to a value of essentially zero for $f\Delta\vec{\mu}_{solute}$. Although the sign of a Kamlet–Taft parameter does not have any physical meaning, it is striking that the same correlation also holds for MeSCN[32,33] (see Table 2). Because $f\Delta\vec{\mu}_{solute}$ is zero for Ac5CNTrp, one may conclude that the nitrile vibration is not sensitive to the local electrostatics, but it is predominantly sensitive to HB interactions (see the blueshifted absorption in protic HFIP in Fig. 3D).

More data are required to be collected for different compounds to ascertain if this correlation still holds. Alternatively, a theoretical approach such as that described by Błasiak *et al.*[44] may reveal the links between the molecular environment and the observed solvatochromism. Based on the results presented here, 4CNTrp is more promising than 5CNTrp as a local vibrational probe for changes in electrostatics as well as HB interactions.

In addition to the steady-state IR absorption experiments, we also undertook ultrafast time-resolved studies in order to determine the vibrational lifetime and to investigate if it is modulated by the local environment. In Fig. 4, the results of a global analysis are shown after applying a fit consisting of a sum of exponentials to the data. The negative bleach feature in the difference spectra arises due to a depopulation of the vibrational ground state, and the positive one arises from an induced absorption of the first vibrationally excited state (ESA). The ESA feature vanishes on a picosecond time scale due to vibrational relaxation, and it is replaced by an induced absorption at only a slightly lower wavenumber with respect to the vibrational ground state, which is a typical signature of a hot ground state. The lifetimes of all compounds are only weakly solvent-dependent (1.4–1.9 ps) and similar to values found for other CN stretch vibrations such as that of 3-methyl-5CI (1.8 ps in DMSO/TFE),[34] benzonitrile (4 ps in DMSO,[45] 3 ps in methanol[46]), 4CNphenol (1.5 ps in methanol),[47] and cinnamonitrile (3 ps in methanol).[46] A lifetime of 1.4–1.9 ps theoretically corresponds to a 3.4–2.5 cm^{-1} wide Lorentzian. The larger linewidth of 8–26 cm^{-1} that we observe in the FTIR spectra can therefore be attributed to inhomogeneous broadening. The 'slow' observed absorption difference spectra (with time constants of 10 ps up to long-lived, *i.e.* signals that persist for times longer than our longest measured 150 ps delay time) are signs of solvent heating. The short vibrational lifetime limits the potential application of the CN-substituted Trp analogs as labels for 2D-IR spectroscopy and renders them more suitable for steady-state applications such as FTIR or regular time-resolved IR spectroscopies. In agreement with the absorption spectra shown in Fig. 2C, 4CNI shows two bleaches. Only one broad ESA feature is found, however, potentially containing contributions of both ground state bleaches. Two clearly separated ESA features are, however, reported in isopropanol.[35] For completeness, the time evolution of the measured raw maximum and minimum (difference) absorption signals and their global fits are shown in the ESI† (Fig. S1).

UV-vis and fluorescence properties

In analogy with the Kamlet–Taft relationship used above to describe the observed IR shifts, commonly used theoretical models for emission shifts, such as the Ooshika–Lippert–Mataga model, are also only capable of modeling unspecific interactions (*e.g.* disregarding HB interactions and ignoring effects due to solvent molecules having a finite size).[48,49] In protic solvents where specific solvent–solute interactions occur, the Stokes shift is typically larger than predicted.[50,51]

The absorption spectra of the 5CN analogs show a main peak at around 280 nm and for those of the 4CN analogs, at around 305 nm (see Fig. 5). For all compounds, three characteristic solvents are chosen because they represent a low polarity (THF), a high polarity (DMSO), and a HB forming + high polarity (water) environment. The corresponding emission spectra show a solvent-dependent Stokes shift, which classifies cyanoindoles, like tryptophan, as fluorescent probes that are

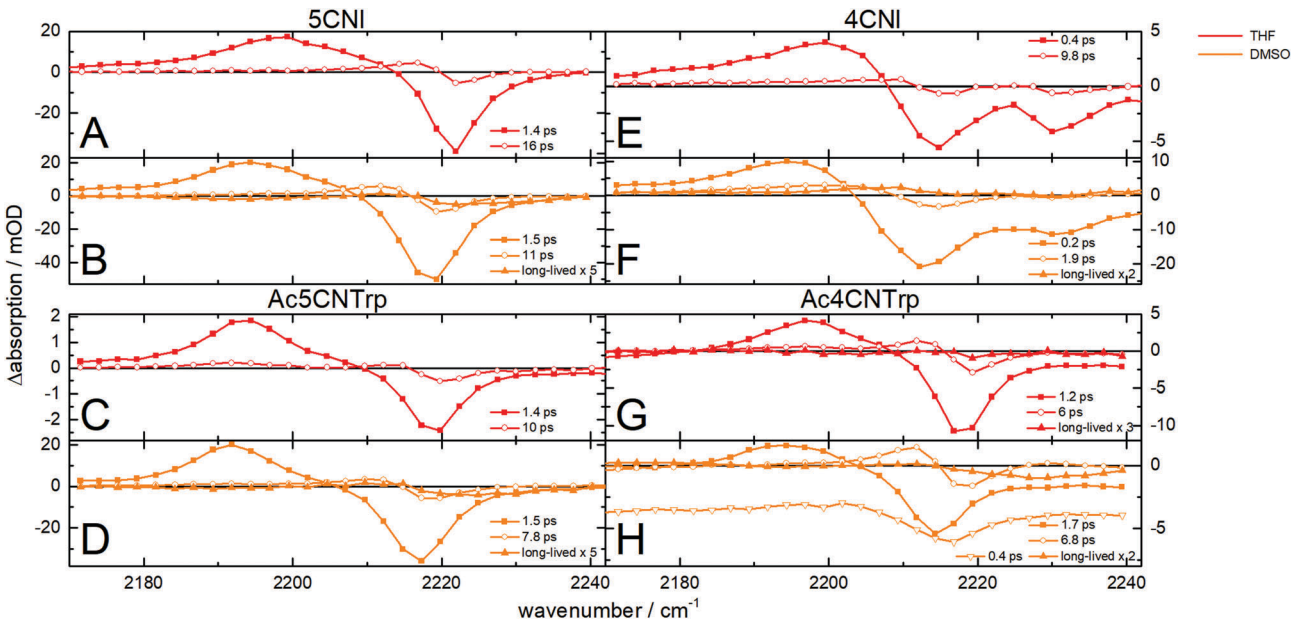

Fig. 4 Ultrafast time-resolved IR experiments. The spectra of 5CNI (panels A and B; each compound is measured in THF and in DMSO, shown in the top and bottom panels, respectively), Ac5CNTrp (C and D), 4CNI (E and F), and Ac4CNTrp (G and H) are a result of a global analysis, after applying a sequential model. Each spectrum has an associated lifetime, which is given in the legend. The spectra collected in the same solvent have the same colour coding (see the legend outside panel E) but different symbols (which represent the data points).

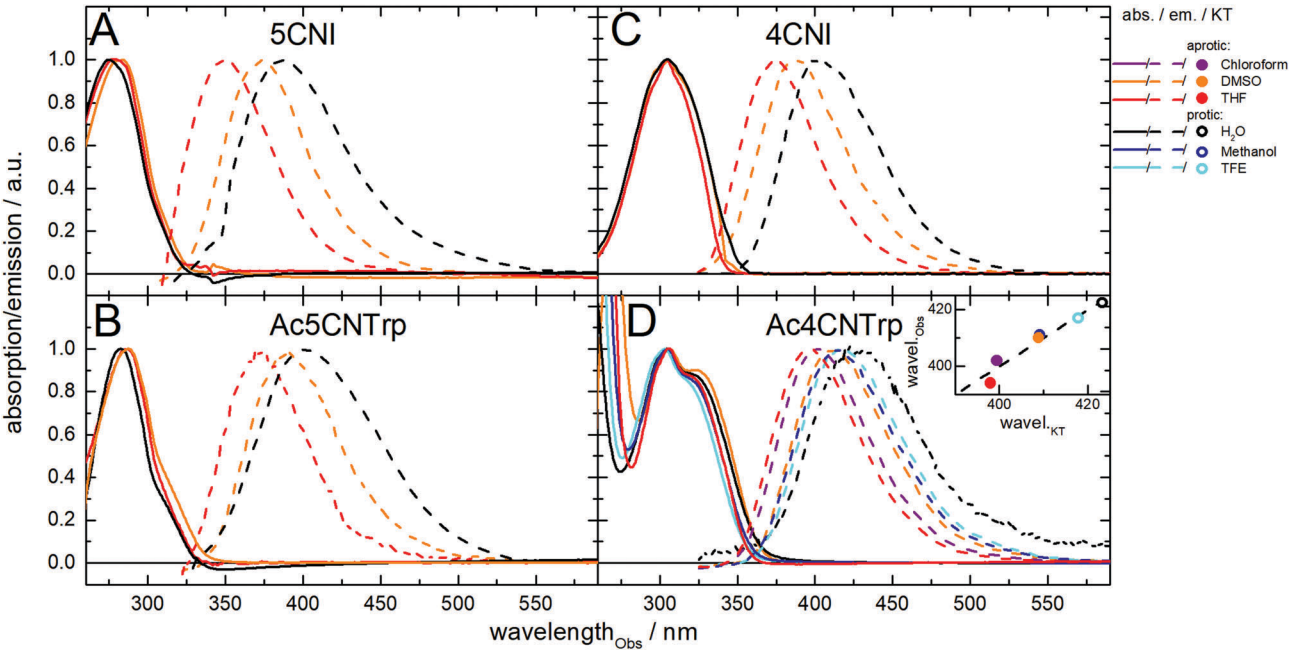

Fig. 5 Normalized absorbance and emission spectra of all compounds. The emission is collected after excitation at 310 nm and shown beyond 310 nm (A), 320 nm (B) and 325 nm (C and D). The inset in panel D shows the predicted Kamlet–Taft emission wavelengths as a function of the observed emission at its maximum (with $\Delta\lambda$ (nm) = 383 + 11·α + 1.8·β + 25·π*; R^2 = 0.95). The values used for the Kamlet–Taft model are the maxima of the corresponding spectra. The diagonal is shown as a guide to the eye. All panels share the same legend with each solvent having the same colour.

sensitive to their surroundings. The Stokes shift is also visualized in the inset of panel D where the maximum emission wavelengths are plotted against the theoretical Kamlet–Taft wavenumber. Because this model requires 4 parameters for a unique solution, only Ac4CNTrp is modelled (Fig. 5D). The fluorescence quantum yields have also been determined (see Table 3). A comparison to a selection of literature values[18,22,52] is presented in Table S2 (ESI†). Including an additional fast 1 ps component to the fits (to account for potential instantaneous scatter) did not significantly change the time constants shown in Table 3. The 4CN analogs have a significantly higher quantum yield than the 5CN analogs, rendering the nitrile at the 4 position a more efficient fluorescent probe. For example, Ac4CNTrp is found to have a quantum yield at least two orders of magnitude higher in H_2O than that found for Ac5CNTrp.

The solvent environment influences not only the Stokes shift of the studied compounds, but also the electronic lifetimes (and the quantum yield). In Fig. 6, the collected TCSPC signals

Table 3 Fluorescence properties (quantum yield (QY) and lifetimes) of the studied compounds, determined upon excitation at 310 nm and emission at wavelengths >320 nm. The listed lifetimes are determined *via* a fit to a sum of exponentials, with the standard deviation given in brackets, the fractional intensity of each component in percent, and the goodness-of-fit parameter χ^2. Table S2 (ESI) also lists the intensity-averaged lifetimes

			Lifetimes (error)/ns\fractional intensity/%			
Compound	Solvent	QY	τ_1	τ_2	τ_3	χ^2
5CNI	THF	0.11			4.08 (0.01)\100	1.14
	DMSO	0.16			7.15 (0.02)\100	1.20
	H_2O	<0.01	0.240 (0.003)\32	1.83 (0.04)\24	6.6 (0.2)\43	1.01
Ac5CNTrp	THF	0.09		2.02 (0.01)\4	5.99 (0.02)\96	1.16
	DMSO	0.23		3.5 (0.3)\2	14.60 (0.03)\98	1.16
	H_2O	<0.01		0.340(0.003)\57	5.25 (0.07)\43	1.22
4CNI	THF	0.48			5.00 (0.01)\100	1.09
	DMSO	0.56			7.40 (0.02)\100	1.11
	H_2O	0.59			8.90 (0.02)\100	1.28
Ac4CNTrp	THF	0.44		2.60 (0.09)\5	7.89 (0.02)\95	1.09
	DMSO	0.58		2.13 (0.09)\6	10.17 (0.03)\94	1.24
	H_2O	0.76		4.4 (0.3)\4	13.90 (0.03)\96	1.15
	Chloroform	0.45		2.08 (0.05)\5	6.19 (0.02)\95	1.14
	Methanol	0.55		2.8 (0.2)\13	9.00 (0.02)\87	1.21
	TFE	0.76		2.6 (0.1)\5	10.03 (0.02)\95	1.47

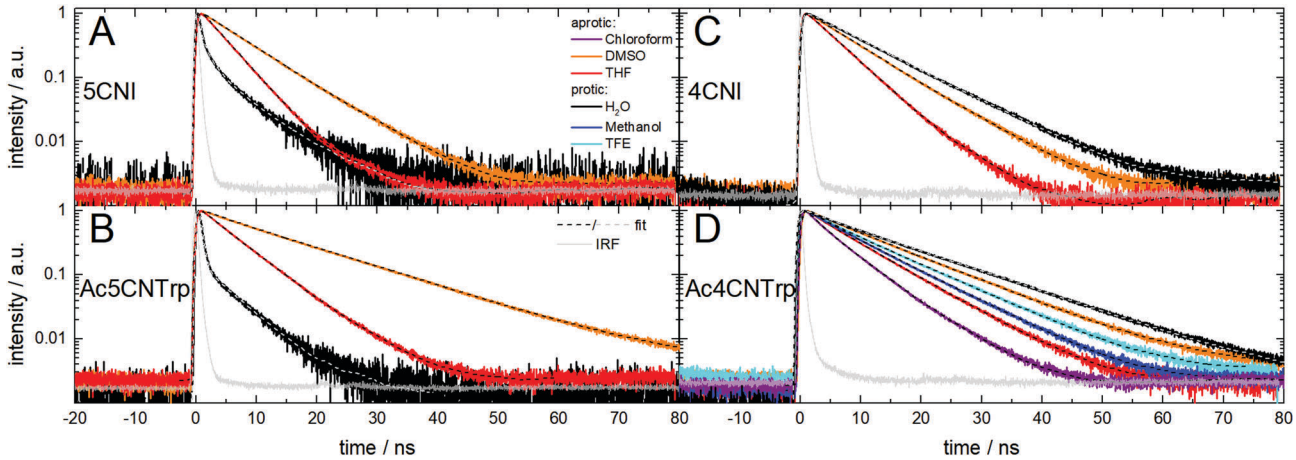

Fig. 6 Normalized time-resolved fluorescence emission decays of all compounds in different solvents. For each curve, their multi-exponential fits are shown (see Table 3 for the fitted lifetimes). For clarity, the dashed fit is coloured grey in water, otherwise black is used. The grey curve represents a typical instrument response curve (IRF) as collected in each solvent on a reference (TiO_2) measurement. The raw data (with residuals) are shown in Fig. S2 (ESI†).

are presented, which are integrated at wavelengths greater than 320 nm. The lifetimes fitted to the decay curves are given in Table 3. The lifetimes are consistent with literature values for related compounds (see Table S2, ESI†).[18,22,53]

The indoles (4CNI and 5CNI) generally exhibit single exponential lifetimes while the other compounds exhibit two or three. Trp typically exhibits two or three (excitation-independent) fluorescence lifetimes, which seem to be inherent in its structure and are attributed to two nearly identical electronic absorption transitions (having different excited-state dipole moments and HB interaction sensitivities), or, alternatively, to structural heterogeneity (*i.e.* different rotamers).[54,55]

Water quenches the fluorescence of both 5CN analogs, as evidenced by their low quantum yields. The lifetime in water can be more accurately measured for the 4CN analogs, where the quantum yield is much higher. Here, we see that a more polar environment extends the electronic lifetime. A similar trend is also seen for Ac4CNTrp (of which we have most data at hand), as depicted in Fig. 7. Sorting the nanosecond lifetimes by size and fitting them to a linear function, we find a positive slope Δ.

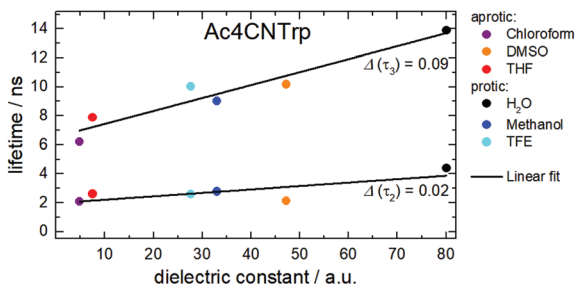

Fig. 7 The electronic lifetime of Ac4CNTrp depends on the dielectric constant. The lifetimes τ_2 and τ_3 listed in Table 3 exhibit two clearly distinct correlated clusters of datapoints. Both lifetime clusters are fitted separately to a linear relationship with slope Δ (depicted near each line). Fig. S3 also shows the fit to the intensity-averaged lifetimes listed in Table S2 (ESI†), resulting in the same slope as observed for the slow components.

The observed changes in lifetime (and the quantum yield) clearly render the labels useful as protein markers as they are capable of reporting changes in their local environment.

Conclusions

CN-substituted Trp analogs are versatile probes for local electrostatics and HB interactions, which can be applied both for static and dynamics measurements. Our detailed studies characterize the IR and UV/visible spectroscopic properties. Taken together, these chromophores can be used as reporters of changes in their local environment on time scales ranging from femtoseconds (*e.g.* in vis-pump IR-probe or 2D-IR spectral diffusion experiments) to infinity (*i.e.* in steady-state experiments). In the IR region, the model compound 4CNI shows two absorption features in the nitrile stretch region, which disappear for the label Ac4CNTrp having an additional substitution on the indole ring system, considerably simplifying the interpretation of the solvatochromic shifts and opening up its use as a vibrational probe in protein studies. In addition, Ac4CNTrp exhibits a large IR $f\Delta\vec{\mu}_{\mathrm{solute}}$ proportionality constant (*i.e.* a high sensitivity of the IR wavenumber to changes in electrostatics). These properties, together with the high fluorescence quantum yield, make 4CNTrp a very promising dual label. Ac5CNTrp, on the other hand, exhibits essentially a zero $f\Delta\vec{\mu}_{\mathrm{solute}}$ proportionality constant. This fact renders it as a suitable IR marker for HB interactions. Depending on the intended application, all compounds can thus serve as useful local probes, although their use as an ultrafast 2D-IR label in spectral diffusion measurements is relatively limited due to their short (<2 ps) vibrational lifetimes. On slower time scales, the long fluorescence lifetime can be exploited (*i.e.* tens of nanoseconds). Not only is their fluorescence useful on 'intermediate' and longer time scales, they can be used as vibrational labels as well in transient experiments (*e.g.* photoswitchable proteins or protein folding). In that fashion, the fluorescence or IR spectral properties can be tracked as a

function of time (from femtoseconds to open-end) after protein dynamics has been initiated. Both the IR and fluorescence properties can then provide valuable information on changes in local electrostatics and HB status. Probing different parts of the electromagnetic spectrum (and their associated time scales) may thus be used to address and access different structural dynamics phenomena in proteins.

Conflicts of interest

There are no conflicts to declare.

Acknowledgements

The authors gratefully acknowledge the Deutsche Forschungsgemeinschaft for funding through INST 161/722-1 FUGG and GRK 1986, and the Alexander von Humboldt Foundation for a Sofia Kovalevskaja Award.

References

1 J. M. Beechem and L. Brand, *Annu. Rev. Biochem.*, 1985, **54**, 43–71.
2 C. A. Royer, *Chem. Rev.*, 2006, **106**, 1769–1784.
3 P. C. Callis, *J. Mol. Struct.*, 2014, **1077**, 22–29.
4 S. Bobone, M. van de Weert and L. Stella, *J. Mol. Struct.*, 2014, **1077**, 68–76.
5 S. P. Narayanan, A. Maeno, H. Matsuo, M. Oda, H. Morii and K. Akasaka, *Biophys. J.*, 2012, **102**, L8–L10.
6 M. Hospes, J. Hendriks and K. J. Hellingwerf, *Photochem. Photobiol. Sci.*, 2013, **12**, 479–488.
7 P. Singh and P. K. Chowdhury, *J. Phys. Chem. B*, 2017, **121**, 4687–4699.
8 J. Broos, H. H. Pas and G. T. Robillard, *J. Am. Chem. Soc.*, 2002, **124**, 6812–6813.
9 A. B. T. Ghisaidoobe and S. J. Chung, *Int. J. Mol. Sci.*, 2014, **15**, 22518–22538.
10 H. Sahoo, D. Roccatano, M. Zacharias and W. M. Nau, *J. Am. Chem. Soc.*, 2006, **128**, 8118–8119.
11 J. D. Slocum and L. J. Webb, *J. Am. Chem. Soc.*, 2016, **138**, 6561–6570.
12 M. M. Waegele, R. M. Culik and F. Gai, *J. Phys. Chem. Lett.*, 2011, **2**, 2598–2609.
13 H. Taskent-Sezgin, J. Chung, V. Patsalo, S. J. Miyake-Stoner, A. M. Miller, S. H. Brewer, R. A. Mehl, D. F. Green, D. P. Raleigh and I. Carrico, *Biochemistry*, 2009, **48**, 9040–9046.
14 M. J. Tucker, R. Oyola and F. Gai, *Biopolymers*, 2006, **83**, 571–576.
15 S. Bobone, M. de Zotti, A. Bortolotti, B. Biondi, G. Ballano, A. Palleschi, C. Toniolo, F. Formaggio and L. Stella, *Biopolymers*, 2015, **104**, 521–532.
16 J. Ma, I. M. Pazos, W. Zhang, R. M. Culik and F. Gai, *Annu. Rev. Phys. Chem.*, 2015, **66**, 357–377.
17 X. Chen and Y.-W. Wu, *Org. Biomol. Chem.*, 2016, **14**, 5417–5439.
18 B. N. Markiewicz, D. Mukherjee, T. Troxler and F. Gai, *J. Phys. Chem. B*, 2016, **120**, 936–944.
19 P. Talukder, S. Chen, B. Roy, P. Yakovchuk, M. M. Spiering, M. P. Alam, M. M. Madathil, C. Bhattacharya, S. J. Benkovic and S. M. Hecht, *Biochemistry*, 2015, **54**, 7457–7469.
20 M. R. Hilaire, D. Mukherjee, T. Troxler and F. Gai, *Chem. Phys. Lett.*, 2017, **685**, 133–138.
21 J.-H. Choi, K.-I. Oh, H. Lee, C. Lee and M. Cho, *J. Chem. Phys.*, 2008, **128**, 134506.
22 M. R. Hilaire, I. A. Ahmed, C.-W. Lin, H. Jo, W. F. DeGrado and F. Gai, *Proc. Natl. Acad. Sci. U. S. A.*, 2017, **114**, 6005–6009.
23 M. M. Waegele, M. J. Tucker and F. Gai, *Chem. Phys. Lett.*, 2009, **478**, 249–253.
24 J. B. Alexander Ross, E. Rusinova, L. A. Luck and K. W. Rousslang, in *Topics in Fluorescence Spectroscopy, Volume 6: Protein Fluorescence*, ed. J. R. Lakowicz, Kluwer Academic Publishers, Boston, MA, 2002, pp. 17–42.
25 N. Budisa, *Angew. Chem., Int. Ed.*, 2004, **43**, 6426–6463.
26 J. Broos, *Methods Mol. Biol.*, 2014, **1076**, 359–370.
27 G. Blaser, J. M. Sanderson, A. S. Batsanov and J. A. K. Howard, *Tetrahedron Lett.*, 2008, **49**, 2795–2798.
28 Y. Yokoyama, H. Hikawa, M. Mitsuhashi, A. Uyama and Y. Murakami, *Tetrahedron Lett.*, 1999, **40**, 7803–7806.
29 J. Bredenbeck and P. Hamm, *Rev. Sci. Instrum.*, 2003, **74**, 3188–3189.
30 L. J. G. W. van Wilderen, C. N. Lincoln and J. J. van Thor, *PLoS One*, 2011, **6**, e17373.
31 A. J. Reuss, C. Grünewald, M. Braun, J. W. Engels and J. Wachtveitl, *ChemPhysChem*, 2016, **17**, 1369–1376.
32 L. J. G. W. van Wilderen, D. Kern-Michler, H. M. Müller-Werkmeister and J. Bredenbeck, *Phys. Chem. Chem. Phys.*, 2014, **16**, 19643–19653.
33 L. J. G. W. van Wilderen, D. Kern-Michler, H. M. Müller-Werkmeister and J. Bredenbeck, *Phys. Chem. Chem. Phys.*, 2017, **19**, 9676–9678.
34 W. Zhang, B. N. Markiewicz, R. S. Doerksen, A. B. Smith III and F. Gai, *Phys. Chem. Chem. Phys.*, 2016, **18**, 7027–7034.
35 J. M. Rodgers, R. M. Abaskharon, B. Ding, J. Chen, W. Zhang and F. Gai, *Phys. Chem. Chem. Phys.*, 2017, **19**, 16144–16150.
36 *CRC Handbook of chemistry and physics. A ready-reference book of chemical and physical data*, ed. D. R. Lide, CRC Press, Boca Raton, Florida, 84th edn, 2003.
37 *Progress in Physical Organic Chemistry*, ed. R. W. Taft, John Wiley & Sons, Inc., Hoboken, NJ, USA, 1981.
38 M. J. Kamlet, J. L. M. Abboud, M. H. Abraham and R. W. Taft, *J. Org. Chem.*, 1983, **48**, 2877–2887.
39 D. W. Pierce and S. G. Boxer, *Biophys. J.*, 1995, **68**, 1583–1591.
40 L. Onsager, *J. Am. Chem. Soc.*, 1936, **58**, 1486–1493.
41 N. M. Levinson, S. D. Fried and S. G. Boxer, *J. Phys. Chem. B*, 2012, **116**, 10470–10476.
42 T. L. McMeekin, M. L. Groves and N. J. Hipp, in *Amino acids and serum proteins*, ed. R. J. Block and J. A. Stekol, American Chemical Society, Washington, D.C., 1964, vol. 44, pp. 54–66.
43 C. L. Yaws, *The Yaws handbook of physical properties for hydrocarbons and chemicals*, Elsevier Science GPP, Amsterdam, 2nd edn, 2015.
44 B. Błasiak, A. W. Ritchie, L. J. Webb and M. Cho, *Phys. Chem. Chem. Phys.*, 2016, **18**, 18094–18111.

45 M. Banno, A. Kotani, K. Ohta and K. Tominaga, *Bull. Chem. Soc. Jpn.*, 2014, **87**, 470–478.
46 A. Ghosh, A. Remorino, M. J. Tucker and R. M. Hochstrasser, *Chem. Phys. Lett.*, 2009, **469**, 325–330.
47 J.-H. Ha, K.-K. Lee, K.-H. Park, J.-H. Choi, S.-J. Jeon and M. Cho, *J. Chem. Phys.*, 2009, **130**, 204509.
48 E. Lippert, *Ber. Bunsen-Ges.*, 1957, **61**, 962–975.
49 N. Mataga, Y. Kaifu and M. Koizumi, *Bull. Chem. Soc. Jpn.*, 1956, **29**, 465–470.
50 H. M. Rosenberg and E. Eimutis, *Spectrochim. Acta*, 1966, **22**, 1751–1757.
51 T. C. Werner and R. M. Hoffman, *J. Phys. Chem.*, 1973, **77**, 1611–1615.
52 R. F. Chen, *Anal. Lett.*, 1967, **1**, 35–42.
53 J. R. Lakowicz, *Principles of Fluorescence Spectroscopy*, Springer US, Boston, MA, 3rd edn, 2006.
54 J. R. Albani, *J. Fluoresc.*, 2014, **24**, 93–104.
55 J. R. Albani, *J. Fluoresc.*, 2014, **24**, 105–117.